High-throughput dielectrophoretic filtration of sub-micron and micro particles in macroscopic porous materials

Malte Lorenz[*], Daniel Malangré[⁑], Fei Du[*], Michael Baune[*], Jorg Thöming[*, †], Georg R. Pesch[*, †, ‡]

[*] University of Bremen and Center for Environmental Research and Sustainable Technology (UFT), Chemical Process Engineering (CVT), Leobener Str. 6, 28359 Bremen, Germany.

[⁑] University of Bremen and Center of Applied Space Technology and Microgravity (ZARM), Am Fallturm, 28359 Bremen, Germany.

[†] MAPEX Center for Materials and Processes, University of Bremen, Bremen, Germany.

[‡] Corresponding author (email: gpesch@uni-bremen.de).

Acknowledgements

M. Lorenz thanks Arne-Brün Vogelsang (University of Bremen) for assisting in experimental work, Michael Birkner (workshop, University of Bremen) for manufacturing the filtration cell, Oliver Focke (Hybrid Materials Interfaces Group, University of Bremen) for taking CT scans of the porous filter materials and Thomas Ilzig (Chair of Magnetofluiddynamics, Measurement and Automation Technology, Dresden University of Technology) for his introduction into image-based filter structure characterization. M. Lorenz would further like to thank Benjamin Besser (Center for Environmental Research and Sustainable Technology, University of Bremen) for providing the graphite particle dispersion.

Author Contributions

M. Lorenz, G. Pesch, F. Du, M. Baune, and J. Thöming conceived the experiments. M. Lorenz conducted the experiments. D. Malangrè provided the porous ceramic samples. M. Lorenz, G. Pesch, F. Du, M. Baune, and J. Thöming analyzed the results. G. Pesch and M. Baune supervised the project. M. Lorenz wrote the manuscript with input from all other authors.

Funding

This work was supported by the German Research Foundation (DFG) through the research training group “Micro-, Meso-, and Macroporous non-metallic Materials: Fundamentals and Applications” [GRK 1860], the priority program SPP2045 “MehrDimPart” [TH 893/20-1], and the Federal Ministry for Economic Affairs and Energy (BMWi), Germany, through the project “Joint research project for the development of combustion technologies in the CEC for climate friendly energy generation; Basics, Improvement of damping properties of ceramic combustion chamber liners” [03ET7011S].

Abstract

State-of-the-art dielectrophoretic (DEP) separation techniques provide unique properties to separate particles from a liquid or particles with different properties such as material, morphology or size from each other. However, such separators do not operate at throughput that is sufficient for a vast fraction of separation tasks. The reason for this limitation is that, in order to move particles by dielectrophoresis, high electric field gradients to drive the separation are required. Conventionally, those gradients are generated by electrode microstructures that limit the maximum channel size. Here, we investigate DEP filtration, a technique that uses open porous microstructures instead of microfluidic devices to easily increase the filter cross section and therefore also the processable throughput by several orders of magnitude. Previously, we already separated baker's yeast by DEP filtration in open porous ceramic structures. Now, we give a more elaborate experimental study about DEP filtration in these open porous structures and separate model particles, that are an order of magnitude smaller (500 nm, polystyrene), from aqueous suspensions. Almost 100% separation at flow rates of up to 9 mL min^{-1} was achieved while the majority of the trapped particles could be recovered. We show how particle separation depends on key parameters (voltage, throughput, filter structure size). Further, we work towards selective particle separation and show that particle separation is very dependent on the particle polarizability: This creates the possibility to adjust selectivity by changing the electrical conductivity of the suspension around that of the particle. This study highlights the unique qualities of dielectrophoretic filtration enabling switchable, selective, and scalable particle separation to solve existing problems such as cell separation or precious metal recovery.

I. INTRODUCTION

Separation of micron and sub-micron particles from liquid media or according to their properties is essential for a wide variety of fields. It is key for bio analytics, medical diagnostics [1], as well as product purification [2], for recovery and mining of valuable materials [3]–[5], or to increase the sustainability and cost efficiency of industrial processes. A pressing biomedical challenge is the detection of circulating tumor cells (CTC) in blood which is important for prognosis during treatment of various cancers [6]. The concentration of CTC in blood, however, is in the range of 10^{-3} ppm which makes them challenging to find and concentrate. A complementing technical example is the recovery of precious materials from electronic waste. One of the first steps during this process is to shred down the electronic waste to small pieces to then use standard physical separation processes for material recovery, for example based on differences in density or magnetism. Noble metals are concentrated in the fine dust that is produced as byproduct during milling and 10 to 35% of the total amount of noble metals are currently lost because of inefficient separation processes for this fraction [5], [7]. A separation technique to recover these valuable particles from the dust would allow us to mine otherwise lost materials from waste. Currently available separation techniques, such as deep bed filtration and centrifugation, are used to separate particle systems according to size or density but at small particle scales (of the dimension of cells or fine dust) density separation fails as the weight differences become negligible and size exclusion mechanisms require high pressure differences to achieve significant throughputs. Thus, different approaches are required.

Dielectrophoresis (DEP) is an electrokinetic phenomenon that can be exploited for highly selective separation techniques [8]. It was for example applied to separate target cells/particles against millions of background particles [9], live and dead cells [10], blood cells according to type, and circulating tumor cells from whole blood [1], [11]–[13]. However, most DEP-based separators require microfluidic devices and lack the capability to process sufficiently high throughputs to handle separation tasks at industrial or preparative scale. The reason for why these separators offer high selectivity but limited throughput lies in the inherent physics of DEP.

DEP-based separation techniques utilize spatially non-uniform electric fields to move polarizable particles [14]. The DEP force depends on the particle volume, its relative polarizability, and the spatial change of the electric field. Using the point-dipole approximation, the DEP force $\langle \mathbf{F}_{\mathrm{DEP}} \rangle$ can be expressed as

$$\langle \mathbf{F}_{\mathrm{DEP}} \rangle = \frac{1}{4} \pi d_{\mathrm{P}}^3 \mathrm{Re}[K] \nabla |\mathbf{E}_{\mathrm{RMS}}|^2 \tag{1}$$

with, the del operator $\nabla = (\partial/\partial x, \partial/\partial y, \partial/\partial z)$, which gives the gradient of a scalar field, the particle diameter d_{P}, the real part of the complex Clausius-Mossotti (CM) factor $\mathrm{Re}[K]$, and the root-mean-square electric field vector $\mathbf{E}_{\mathrm{RMS}}$. The real part of the CM factor $\mathrm{Re}[K]$ describes the relative electric polarizability of a particle with respect to the surrounding medium and represents the reason why DEP can be applied for selective particle separation according to dielectric properties. The CM factor depends on the complex permittivities of the particle, $\tilde{\varepsilon}_{\mathrm{P}}$, and the medium the particle is suspended in, $\tilde{\varepsilon}_{\mathrm{m}}$, and its real part is given by

$$\mathrm{Re}[K] = \mathrm{Re}\left[\frac{\tilde{\varepsilon}_{\mathrm{P}} - \tilde{\varepsilon}_{\mathrm{m}}}{\tilde{\varepsilon}_{\mathrm{P}} + 2\tilde{\varepsilon}_{\mathrm{m}}}\right]. \tag{2}$$

The complex permittivity describes the frequency (ω)-dependent polarizability of a material and is dependent on the material's permittivity ε and conductivity σ, $\tilde{\varepsilon} = \varepsilon + j\frac{\sigma}{\omega}$. At low field frequencies particle polarization is only dependent on the electrical conductivity of the particle, σ_P, and the surrounding medium, σ_m, and the real part of the CM factor becomes

$$\mathrm{Re}[K] = \frac{\sigma_\mathrm{P} - \sigma_\mathrm{m}}{\sigma_\mathrm{P} + 2\sigma_\mathrm{m}} \tag{3}$$

because the majority of the charge that causes polarization is transferred by conduction [15]. At high frequencies, this mechanism changes because the time for charges to align with the field due to conduction is too short and polarization occurs due to molecular polarization mechanisms (which is expressed through the permittivities of the particle and medium). $\mathrm{Re}[K]$ can take values between 1 and –0.5 and the sign dictates if particles will move along or against the electric field gradient; this allows to move particles of different polarizability (different dielectric signature) to opposite directions in the field gradient. If the particle is more polarizable than the surrounding medium, the CM factor will be positive and the particle will experience positive dielectrophoresis (pDEP) resulting in a force pointing towards higher electric field regions (with the field gradient). On the other hand, if a particle is less polarizable, the CM factor is negative, the particle will experience negative dielectrophoresis (nDEP) and the acting force points towards low electric field regions (against the field gradient). There are numerous approaches to use this effect for selective particle separation. Dielectrophoresis is for example used in microchannels to continuously separate particles of different properties towards different stream lines which directs them to different exits [16]. Dielectrophoresis is also used to attract and trap particles of certain properties at electric field maxima whereas other particles are repelled from those zones [17]. Other DEP-based separation techniques apply additional forces (like electrophoretic or drag forces) to trap the types of particles that experience dominant DEP forces (against the additional forces) while all other particles are still free to move on. Such an approach is for example used in insulator-based DEP techniques [18].

Most DEP-based studies show high selectivity performed in microfluidic devices for diagnostic or analysis at the expense of low throughputs in the range of mL h^{-1} that are only suited for handling very small samples. The reason for that comes from the DEP-force dependence on the electric field gradient. This is why in traditional electrode-based DEP devices the separation efficiency is coupled to the device dimensions: Small distances between the electrodes and thus small channel sizes are required to generate sufficient electric field gradients [15]. In microfluidic devices the channel height is further restricted due to the fabrication limiting the cross section and therefore the throughput of these devices.

Bridging the gap from low- to high-throughput dielectrophoretic applications is an unexplored challenge that our group has focused on [17], [19]–[21]. One way to increase the throughput is to increase the device's cross section as it is done in dielectrophoretic filtration. In this approach, the electric field gradients are not generated by a highly asymmetrical and small electrode design, but porous microstructures are used to disturb an originally homogeneous electric field that is generated by two macroscopic electrodes. The electric field gradient is therefore mainly dependent on the design of the porous microstructure [21], [22], whereas the electrode distance can be increased by several orders of magnitude (centimeter and above) as long as the voltage is increased by the same factor. The dielectrophoretic filtration technique uses the inhomogeneous electric fields generated in such microstructures to trap particles from suspensions that are mechanically pumped through them (Figure 1). Since the electric field maxima are primarily located at the interface between fluid and microstructure, particles that experience positive DEP are pulled out of the fast-moving bulk fluid flow towards these interfaces where they are trapped. Particles that experience negative DEP are

pushed away from the interfaces into the fast-moving fluid flow and carried through the structure. The porous microstructure can therefore work as an electrically switchable filter that retains for example particles that are more conductive than the surrounding fluid (that experience positive DEP) but is permeable to particles of lower conductivity than the surrounding fluid (that experience negative DEP).

The few existing studies from other groups on DEP filtration show manifold-increased throughputs compared to microfluidic approaches. For example, DEP filtration was used for separation of yeast cells from water [23]–[25] at moderate flow rates of 6 mL min^{-1}. In older studies it was already shown that metallic ceramic and plastic particles could be filtered dielectrophoretically from nonconductive liquids at flow rates of 1 L min^{-1} [26], [27]. Wakeman and Butt [28] filtered AC dust and PVC particles from oil and achieved filter efficiencies up to 60% at flow rates of 5 L min^{-1}. All of those studies worked phenomenologically and focused on specific separation tasks but did not describe the process in detail. In order to understand and prospectively design separation processes and devices, knowledge about key parameters that influence the trapping in porous structures is required.

With this aim, we recently derived design rules in a proof-of-principle study using a microfluidic chip and applied them in a macroscopic setup [19]. In a macroscopic setup we achieved throughputs of almost 10 mL min^{-1} retaining up to 90% of baker's yeast cells from an aqueous suspension. In the present work, we want to scrutinize this process further and provide a coherent description about limitations and possibilities of DEP filtration in open porous filters. We systematically link the DEP filtration process to the geometry of the underlying microstructure as well as to operational parameters and demonstrate capabilities for selective retention and recovery of particles. We investigate the influence of the key parameters applied voltage, throughput, filter microstructure and fluid electrical conductivity on the filter efficiency. Experiments were performed with model polystyrene (PS) particles and open porous foam ceramics that were sandwiched between two plate electrodes (Figure 1e). Due to their high porosities (80%) and small and highly connected pores (median pore diameter of about 0.5 mm), the foamed ceramic structures provide properties that we expect to be beneficial for DEP filtration, since they have a low resistance for the fluid flow and fine structures to generate highly inhomogeneous electric fields. They are also cheap to produce, very stable, and thus suited for largely scaled-up filter devices. Further, we focus on the unique possibilities that the method provides (Figure 1a-d), which are switchable particle filtration from liquid, selective particle filtration based on the relative polarizability, and recovery of the trapped particles.

Preprints (www.preprints.org) | NOT PEER-REVIEWED | Posted: 4 December 2019 doi:10.20944/preprints201912.0055.v1

Peer-reviewed version available at Analytical and Bioanalytical Chemistry 2020; doi:10.1007/s00216-020-02557-0

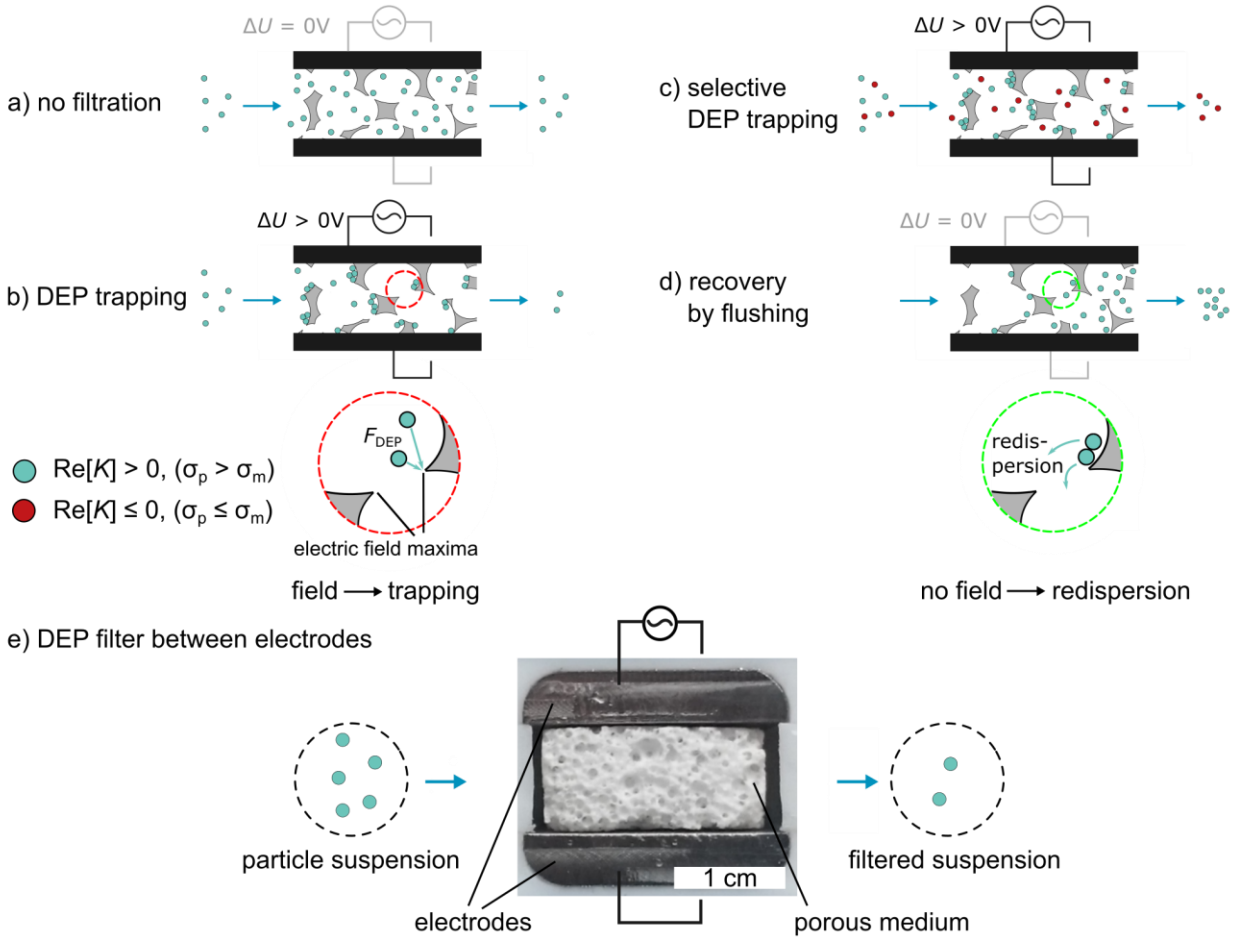

Figure 1: Dielectrophoretic filtration allows switchable particle separation from a liquid or according to particle properties, for example conductivity or size. Particles are pumped through a porous filter medium that is sandwiched between two electrodes. The pore windows of the filter are much bigger than the particle size and thus, the particles will penetrate the filter (follow the flow) when no electric field is applied (a). When an electric field is applied, it will be disturbed by the porous filter resulting in a vast number of electric field maxima and dielectrophoretic particle motion. All particles that are more polarizable (pDEP) than the surrounding medium (blue) are pulled towards the electric field maxima at the filter wall where they are trapped (b). All particles, equal or less polarizable (nDEP) than the medium (red), are not affected or pushed away from the field maxima and thus pass through the filter. This allows to selectively trap particles from particle mixtures (c). When the electric field is switched off the trapped particles are redispersed and can be recovered at higher concentration by flushing the filter (d). The DEP filter (between the electrodes) that was used for experimental study is shown on the bottom (e). The filter has a depth of 2.8 cm and the particle suspension flows from left to right. An image of the whole filter cell is shown in Figure 2a).

II. MATERIALS AND METHODS

Here, we present the experimental setup and procedure used for this manuscript.

A. Particles and particle suspensions

All experiments, except the ones about electrical conductivity-selective particle separation, were conducted using the same particle suspension. Monodisperse carboxylated PS particles with a diameter of 0.5 µm (Polyscience Fluoresbrite, YG Carboxylate Microspheres 0.5 µm) were diluted in ultrapure water that had been degassed under reduced pressure (80 mbar) to a concentration of 2.2×10^6 particles cm^{-3}. A small amount of Tween 20 (0.01 vol%) was added to reduce particle adsorption to the filter. The electrical conductivity was adjusted with KCl to 1.2×10^{-4} S m^{-1}. For the

experiments on electrical conductivity-selective particle separation, we used the same suspension but particles with a diameter of 4.5 µm (Polyscience Fluoresbrite, YG Carboxylate Microspheres 4.5 µm) at a concentration of 2×10^4 particles cm^{-3}. Graphite particles were taken from a graphite water dispersion (Graph Aqua, AMG Graphite GK) with an average diameter of about 3 µm (manufacturer's information). 50 µL of the graphite dispersion were diluted in 500 mL aqueous suspension. The fluid electrical conductivity of the resulting suspension for these experiments was adjusted by adding KCl. For our investigations on electrical conductivity selective particle trapping, it was important to approximate the electrical conductivity of the particles. In general, the particle conductivity can be assumed as a function of its bulk conductivity σ_b, its surface conductance K_s, and its radius a [29]:

$$\sigma_\mathrm{p} = \sigma_\mathrm{b} + \frac{2K_\mathrm{s}}{a}. \quad (4)$$

Since polystyrene is an electrically isolating material the bulk conductivity of a polystyrene particle is negligible and their conductivity is dependent on the double layer that exists at the interface between particle and its surrounding medium. At medium conductivities below 10^{-2} S m^{-1} and particle size equal or above 1 µm diameter, the PS particles conductivity is dominated by the Stern layer conductance which is mainly material dependent and can be assumed as independent of the medium conductivity [30]. With the surface conductance of PS particles which is usually about 1 nS [31], [32], the particle conductivity of a 4.5 µm particle is $\sigma_\mathrm{p,PS} = \frac{2K_\mathrm{s}}{a} = 8.8 \times 10^{-4}\,\mathrm{S\,m^{-1}}$. However, the PS particle conductivity depends a lot on the specific particle and especially its surface [33]. Surface conductivities between 0.2 nS and 2 nS have been reported [30], [32] resulting in a wide range of conductivities between $1.7 \times 10^{-4}\,\mathrm{S\,m^{-1}}$ and to $17 \times 10^{-4}\,\mathrm{S\,m^{-1}}$. Compared to PS particles the conductivity of graphite particles is dominated by their bulk conductivity and was assumed with $\sigma_\mathrm{p,graphite} = \sigma_\mathrm{b} = 3.3 \times 10^2$ to $3 \times 10^5\,\mathrm{S\,m^{-1}}$.

B. Filtration setup

A schematic of the experimental setup is shown in Figure 2a. The volumetric flow of the suspension through the filter cell was controlled between 1 and 11 mL min^{-1} by a peristaltic pump (REGLO Analog, Ismatec). A picture of the filter cell is shown in Figure 1e. It consists of a tapered in- and outlet (to prevent particle accumulation) and the porous filter that is tightly sandwiched in between two stainless steel plate electrodes. A sinusoidal ac voltage between 150 and 600 V_RMS at 1 to 15 kHz was applied across the distance of 8 mm between the electrodes (using a TREK PZD700A power amplifier in combination with a Hameg HM8131 function generator) generating an electric field inside the filter medium perpendicular to the filtrate flow. The power required for DEP in the filter is significantly higher than the power required in microfluidic DEP devices (difference in dimension) which limited the output frequency of our current amplifier to 15 kHz. The replaceable porous filter had a cross section was 8 mm x 29 mm and the filter depth in flow direction was 18 mm. The particle concentration after the filter was determined by using a Fluoromax-4 fluorescence spectrometer (Horiba) and a quartz flow-through cuvette (176.762-QS, Hellma). This allowed us to online detect the fluorescence intensity signals of the filtrate. At the particle concentrations we used in this study, the fluorescence intensity signal is linearly dependent on the particle concentration (as validated by preliminary experiments, not shown) allowing highly accurate particle concentration measurements. The fluorescently labelled particles were excited at a wavelength of 441 nm and emission was detected at 486 nm matching excitation and emission maxima of the particles.

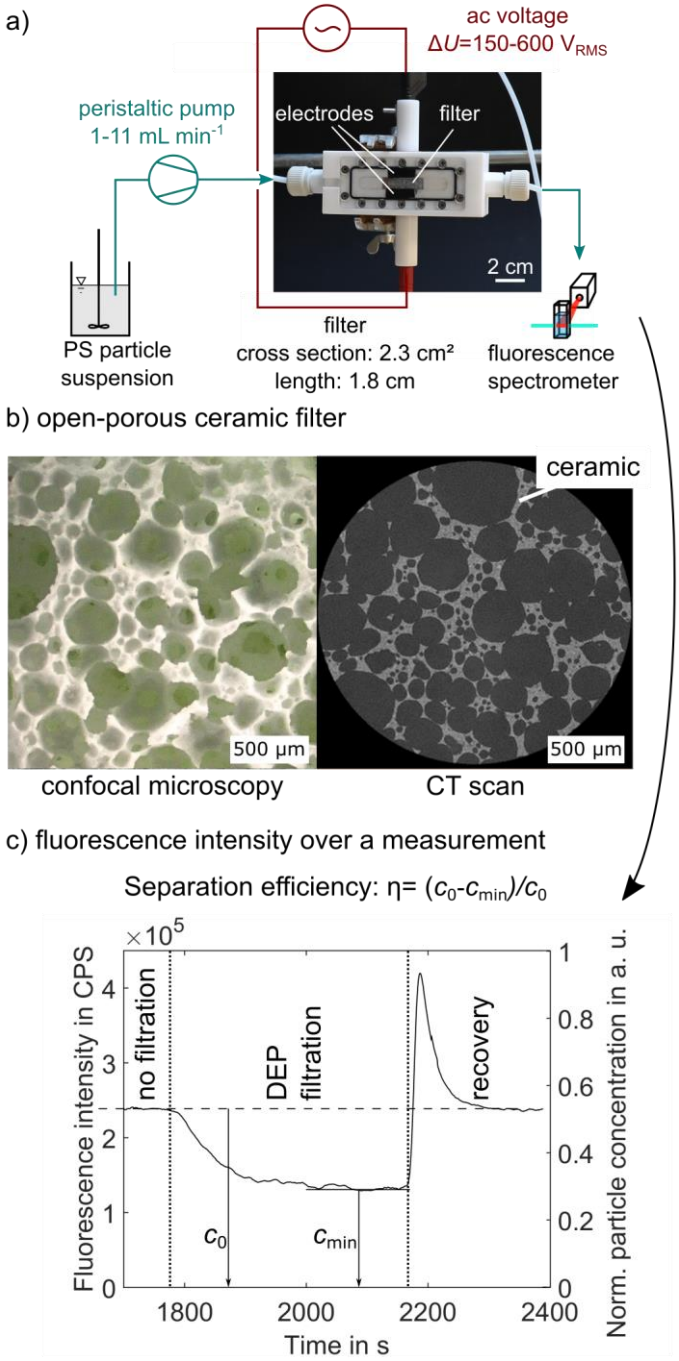

Figure 2: Scheme of the experimental setup with a picture of the filter cell (a). Polystyrene particles were constantly pumped with flow rates from 1 to 11 mL min^{-1} through the porous filter that is sandwiched in between two stainless steel electrodes. The electrodes, that are placed parallel to each other with a distance of 8 mm, were supplied with ac voltages of 150 to 600 V_{RMS} at a frequency between 1 kHz and 15 kHz. The filter has a width of 8 mm, a height of 29 mm, and length (in flow direction) of 18 mm. (b) shows images of the filter structure (confocal microscopy and computed tomography scan). The particle concentration at the outlet of the filter is measured by fluorescence spectroscopy. The fluorescence signal is linearly dependent on the particle concentration and the separation efficiency was defined as $\eta = (c_0\text{-}c_{min})/c_0$. c_0 is the normalized particle concentration when no electric field is applied and c_{min} is the minimum normalized concentration detected when the field is applied. An exemplary plot of the fluorescence intensity in CPS (counts per second)/normalized particle concentration for one measurement cycle is shown in plot (c). In this plot the flow rate during recovery was 5.5 times as high as the flow rate during DEP filtration and the particle recovery rate for this specific experiment was 82%.

C. Porous filter material

The open porous alumina-mullite ceramics were produced by direct foaming. Information about their fabrication are provided in the supplementary materials (section A). Figure 2b shows two exemplary images of the pore structure (a confocal microscope image and one slice from a computed tomography scan). The structure shows spherical pores that are highly connected (highly open porous) by numerous pore windows with sharp thin edges. We used filters with porosities of about 83% and four different structure sizes. The finest structure had a volume-weighed median pore diameter of $d_{pore,3}$ = 280 µm and an area-weighed median pore window diameter of $d_{window,2}$ = 150 µm. The coarsest structure had $d_{pore,3}$ = 760 µm and $d_{window,2}$ = 368 µm, respectively. Pore diameter and pore window diameter were determined from computer tomography data by using MATLAB and the watershed algorithm implemented in the DIPimage package version 2.9. A detailed description of the method is provided in Figure S1 of the supplementary materials.

D. Experimental procedure

All experiments were done with ceramic filters that were used multiple times. To provide constant conditions for each experiment, the setup was flushed with ethanol prior to experiments, to clean the setup and flush out particles and air. Afterwards the setup was flushed with degassed and deionized water to wash out the ethanol. Subsequently the particle suspension was pumped into the setup. To guarantee that the particle suspension at the inlet contained a constant particle concentration, the particle suspension was permanently stirred/dispersed. Each measurement was performed in three steps. 1. Start-up phase. The volumetric flow rate Q was set but no electric field was applied and the particle concentration in the filtrate without dielectrophoretic trapping was determined, c_0 (Figure 2c). 2. DEP trapping phase. The electric field was applied. In response the particle concentration decreased until it reached a constant minimum c_{min}. 3. Recovery phase. The field was switched off and the filter was flushed at the highest flow rate possible Q_{rec} = 11 mL min^{-1}. Flushing was performed with the particle suspension. The particle concentration peaked and then fell slowly back to c_0. We found that the time to reach this minimum concentration was independent of DEP-related parameters. It agreed with the particle retention time in the setup that was determined as the time between injecting a concentration jump at the filter inlet until a constant outlet concentration was reached.

Mechanical trapping. Even with no electric field applied and filter pores and pore windows much bigger than the particles, a small number of particles is remaining in the filter, due to sedimentation and local flow conditions. For each filter the amount of mechanically trapped particles was determined by comparing the particle concentration at the filter outlet (with no electric field applied) to the concentration at the filter inlet. Mechanical trapping of 0.5 µm PS particles was 2%, of 4.5 µm PS particles it was 8% and for graphite it was 22%.

Separation efficiency. The separation efficiency η was defined as the number of particles that was trapped in the filter by the electric field normalized by the amount of particles that entered the filter, $\eta = (c_0\text{-}c_{min})/c_0$.

Particle recovery rate. The particle recovery rate R describes the proportion of dielectrophoretically trapped particles that can be recovered when the electric field is switched off and the filter flushed. The amount of trapped particles was determined by multiplying the temporal integral between c_0 and filter outlet concentration over the time of DEP trapping A_{trap} (Figure 6) with the applied volumetric flow rate Q. The amount of recovered particles was calculated analogously for the time of recovery.

Thus the particle recovery rate was calculated by $R = A_{rec}\, Q_{rec} / (A_{trap}\, Q_{trap})$. The volumetric flow rate for recovering the particles from the filter Q_{rec} was always set to 11 mL min^{-1}.

III. RESULTS AND DISCUSSION

In contrast to our previous study [19] (in which we combined simulation and experiments to scrutinize the trapping of baker's yeast and polystyrene model particles in microchannels and macroscopic filter structures) this study exclusively focuses on experimental DEP filtration in macroscopic structures. Additionally, to an analysis on how the separation efficiency (amount of trapped particles normalized by the total amount of particles that enter the filter) depends on the volumetric flow rate and the voltage, we show the impact of the filter structure. We used fluorescent 500 nm polystyrene beads, which are an order of magnitude smaller than the formerly used baker's yeast, suspended in low-conductive KCl solution and a standard spectrofluorometer in continuous-flow mode. Similarly produced ceramic filters are used, whereas slight variations in the production route cause different pore and pore window sizes (the smallest filter has a volume-weighted median pore diameter $d_{p,3}$ = 320 µm, and an area-weighted median pore window diameter $d_{w,2}$ = 178 µm and was named maliS, the biggest filter has $dp_{,3}$ = 760 µm and $d_{w,2}$ = 368 µm and was named maliXL). We use these filter-size differences to study their influence on particle separation. Further, we will show that the particle polarizability and thus their trapping can be controlled by changing the fluid electrical conductivity and how this indicates that selective separation of particles with different dielectric properties is possible by DEP filtration. Finally, we will attend to particle recovery that can be achieved when switching off the electric field.

A. Influence of volumetric flow rate, applied voltage, and filter structure size

In general, for a given filter structure and a given particle suspension the separation efficiency increases with decreasing volumetric flow rate and increasing applied voltage (Figure 3a). Overall the curves show a smooth but continuous transition between virtually no separation, $\eta = 0.04$ (150 V_{RMS}, 9 mL min^{-1}), and almost complete separation, $\eta = 0.95$ (600 V_{RMS}, 1 mL min^{-1}). Further, when fixing the applied voltage, the separation efficiency is inversely proportional to structure size (Figure 3b). We characterized the filter structure size by their median pore diameter and pore window diameter which do not correlate linearly but follow the same trend. The results show clearly that the separation efficiency is dependent on the structural size, i.e. the inverse of a characteristic pore dimension, of the filter.

The increase in separation efficiency with decreasing volumetric flow rate and increasing applied voltage (Figure 3a) meets our expectations. Simplified, a particle is trapped when it is pulled into a "trapping zone" (i.e., an electric field maximum) where the DEP force dominates over the drag force exerted by the fluid onto the particle. The probability that a particle is trapped (represented by the separation efficiency) is therefore dependent on these two competing forces. From theory we know that the DEP force (Eq. (1)), and thus the DEP migration velocity of the particles, correlates with the applied voltage squared. The volumetric flow rate on the other hand correlates linearly with the superficial velocity and thus the time that a particle has to migrate into a trapping zone.

The separation efficiency is also directly influenced by the dimensions of the filter structure. A decrease in the pore and pore window diameter not only increases the electric field gradients and the number of trapping zones in the filter but also decreases the distance a particle has to travel before it reaches a trapping zone. Pore diameter and pore window diameter are not independent from each

Preprints (www.preprints.org) | NOT PEER-REVIEWED | Posted: 4 December 2019 doi:10.20944/preprints201912.0055.v1

Peer-reviewed version available at Analytical and Bioanalytical Chemistry 2020; doi:10.1007/s00216-020-02557-0

other but follow the same trend. Thus, the influence of pore diameter or pore window diameter cannot be distinguished. However, probably both sizes are relevant for the separation efficiency because small pores lead to a high density of trapping zones and small pore windows generate higher electric field gradients (the field lines must figuratively squeeze through small windows) and thus to higher DEP forces.

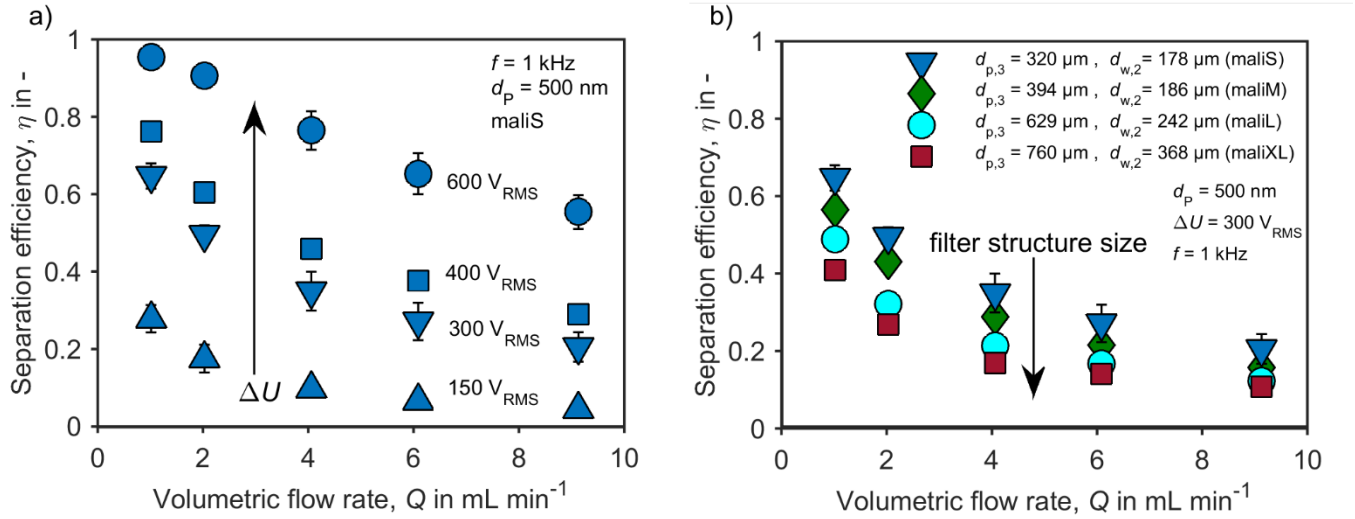

Figure 3: Separation efficiency dependent on the volumetric flow rate and the applied voltage (a) and the filter structure size (b). Each data point represents the average of three measurements. The corresponding standard deviations are given by the error bars.

B. Scaling laws in porous filter materials

In our previous study [19], we introduced scaling laws for DEP trapping in porous filter materials. The respective study was performed with microchannels to model porous structures and we predicted that the separation efficiency in porous structures in general is a function of $\bar{x} = (\Delta U)^2 Q^{-1} d_P^2$. Separation was found to follow $\eta = (1-\exp(\bar{x}/C))$, with C being a fitting coefficient that we used to match experimental results. Figure 4 shows that, when the results from Figure 3 are plotted against $\bar{x}$ they match this prediction remarkably well. In comparison to the separation efficiency achieved in microchannels [19] (dashed line) the results in the porous filter are shifted by five orders of magnitude to the left. Consequently, in the filter $\bar{x} = (\Delta U)^2 Q^{-1} d_P^2$, (which could be interpreted as the cost for operating the process) can be 5 orders of magnitude lower than in the microchannel, to achieve the same separation efficiency. In other words, in the filter we achieve the same separation efficiency at the same applied field strength and particle diameter but at a five orders of magnitude higher volumetric flow rate. For comparability, we transformed the parameter combination of Pesch et al. [19] ($\bar{x} = (\Delta U)^2 Q^{-1} d_P^2 \, h_s \, \mathrm{Re}[K]$) to ours by dividing by the post diameter h_s = 262 µm. The post diameter is comparable to the diameters of the struts in the ceramic filter which vary strongly and have no apparent influence on the separation efficiency. We used a fitting parameter of C = -24.6 10^{-2} V_{RMS} h m^{-1} for the fit through the finest porous filter (maliS). Replacing the finest porous filter by the coarsest (maliXL) led to a horizontal shift by factor two.

An increase in throughput by five orders of magnitude compared to microfluidic applications is a huge step that highlights the potential to increase the throughput of DEP particle trapping by using this or similar porous ceramic filters. To some extend the enhanced separation efficiency can be explained by a roughly 700-fold increase in cross section (230 mm^2) the filter provides over the microchannels (0.336 mm^2) used by Pesch et al. [19]. This means that in principle a 700-fold increase of volumetric flow rate should be possible when increasing the cross section of the

Preprints (www.preprints.org) | NOT PEER-REVIEWED | Posted: 4 December 2019 doi:10.20944/preprints201912.0055.v1

Peer-reviewed version available at Analytical and Bioanalytical Chemistry 2020; doi:10.1007/s00216-020-02557-0

microchannels (e.g., by numbering up). This, however, explains only 3 of the actual 5 orders of magnitude difference. Additionally, the separation efficiency is influenced by the length and especially the tortuosity of the filter that determine the average particle residence time in the filter. The porous filter is approximately twice as long as the microchannels used by Pesch et al. [19] which just explains a factor of two. We conclude that a main reason for the 2 remaining orders of improved trapping efficiency compared to the regular microstructure are the tortuous flow conditions in the porous filter. Since the structure is very inhomogeneous (providing a broad pore size and pore window size distribution and many sharp corners), strong fluid mixing is expected, resulting in an increased particle transport to the trapping zones. Furthermore, in such a randomized structure it is likely that particles have to pass very small pore windows which provide ideal trapping conditions (high electric field gradients and low flow velocities). How beneficial the trapping conditions in the porous filter are becomes even clearer when considering that replacing the finest (maliS) by the coarsest filter structure (maliXL) led to a horizontal shift by only factor two.

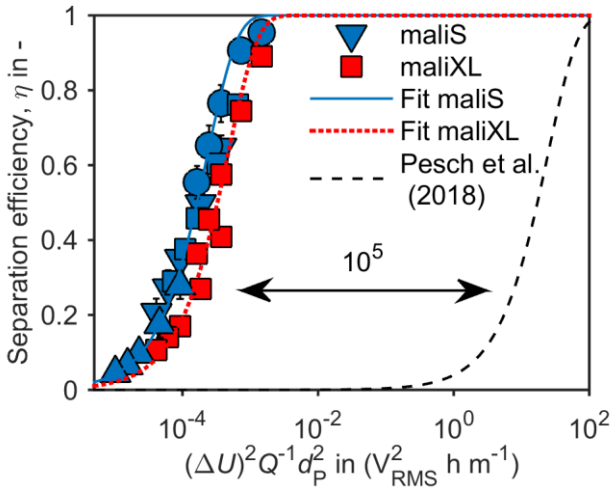

Figure 4: Separation efficiency η as a function of $\bar{x} = (\Delta U)^2 Q^{-1} d_P^2$ for the finest and the coarsest filters, varied voltage ΔU = 150-600 V_{RMS}, and volumetric flow rate Q = 1-9 mL min^{-1} compared to simulated and experimentally validated results of G. R. Pesch et al. (2018) (dashed line). The results for the filter structure maliS (blue) are the ones shown in Figure 3a. Fitting was done using η = (1-exp($\bar{x}/C$)) resulting in C = -24.6 10^{-2} V_{RMS} h m^{-1} (maliS) and C = -49.2 10^{-2} V_{RMS} h m^{-1} (maliXL).

C. Electrical conductivity-selective particle separation

Selectivity in DEP filtration has rarely been investigated before [25]. To show that selective trapping is possible, we investigated how strongly the particle trapping is influenced by the particle's relative polarizability, given by $\mathrm{Re}[K]$ in Eq. (2) and how different relative polarizabilities can be used to separate particles of different type. We already mentioned that at low frequencies $\mathrm{Re}[K]$ is a function of only the conductivities of the particle and the surrounding medium and that it becomes 1 when the particle is much more conductive than the surrounding medium $\sigma_P \gg \sigma_m$ and -0.5 for $\sigma_P \ll \sigma_m$. By changing the medium conductivity in the regime around the particle conductivity, we can therefore adjust the particle polarizability and hence the effective DEP force on the particles that leads to particle separation in the filter.

We investigated this with 4.5 µm PS particles in an aqueous suspension. The conductivity of the suspension was stepwise increased around the particle conductivity (that we estimated to be between 2×10^{-4} S m^{-1} and 16×10^{-4} S m^{-1}) from 1.2×10^{-4} S m^{-1} to 22×10^{-4} S m^{-1}. For a reference, a similar experiment was also performed with highly conductive graphite particles

Preprints (www.preprints.org) | NOT PEER-REVIEWED | Posted: 4 December 2019 doi:10.20944/preprints201912.0055.v1

Peer-reviewed version available at Analytical and Bioanalytical Chemistry 2020; doi:10.1007/s00216-020-02557-0

($\sigma_{graphite} = 33 \times 10^2$ S m^{-1} to 3×10^5 S m^{-1}) with average size of 3 µm. The conductivity of electrically insulating polystyrene particles is dominated by their surface conductivity that exists due to the conductive double layer that forms when the particles are suspended in aqueous suspension. Eq. (4) in Materials & Methods section gives insights into how to derive the overall conductivity from the surface conductance.

PS particles were most-efficiently trapped at the lowest investigated fluid electrical conductivity ($\sigma = 1.2 \times 10^{-4}$ S m^{-1}) with η being around 0.5 (Figure 5). With increasing fluid electrical conductivity, the separation efficiency fell to a minimum of $\eta = 0.1$ at about $\sigma = 4.2 \times 10^{-4}$ S m^{-1} and subsequently increased again to about $\eta = 0.2$. Graphite particles showed a higher separation efficiency of about $\eta = 0.83$ that decreased slowly to $\eta = 0.76$ at $\sigma = 40 \times 10^{-4}$ S m^{-1}.

Particles that are more conductive than the suspension experience positive DEP. They are consequently attracted by the electric field maxima at the filter wall [34] where they are trapped tightly and thus most efficiently. To make sure that the particle trapping at low medium conductivity can be attributed to pDEP, we captured this scenario for 4.5 µm PS particles in microchannels (Figure 4b, the microchannels are the same as used in our previous study, [19]; see Supporting Documents for a comprehensive description of the experiments and channels). The different trapping zones that occur in the microchannels are visualized in Figure 4e. The trapping zones observed at low conductivities as shown in Fig. 4b match the predicted pDEP trapping zones. We can also see that particles that are as conductive as the fluid experience no DEP and the particles are thus randomly dispersed in the suspension (Figure 5c). Consequently, the separation efficiency is lowest (minimum at 4.2×10^{-4} S m^{-1} in Figure 5a) because particles freely follow the flow. When particles are less conductive than the fluid, they experience negative DEP that rejects the particles from the electric field maxima at the traps. In this case, particles can still be trapped, since they are rejected from the pore windows (where the electric field strength is high) or they could become trapped at field minima in the filter. However, negative DEP trapping is expected to be less effective because, as evident from the negative bound of Re[K] of -0.5 compared to the positive bound 1, negative DEP trapping can only be half as strong as positive DEP trapping. Further, the majority of the particles are not tightly trapped at the walls but in the fluid where they are strongly affected by the fluid drag. Also, simulations on microchannels and pillar arrays show that the gradient at field minima is by several orders of magnitude lower than the gradient at field maxima, indicating less holding forces for nDEP trapping. Observations in microchannels (Figure 5d) show that at high medium conductivities particles assemble at nDEP trapping zones where the electric field is lowest.

The results in Figure 5 reflect the theoretical predictions remarkably well. The polystyrene particles show a minimum in separation efficiency at about 4.2×10^{-4} S m^{-1}, which is in a plausible range for their conductivity [30], [32]. The separation results become even clearer when we compare the separation efficiency to the particle polarizability. A calculation of the absolute value of the particle polarizability represented by Re[K] (Eq. (3)) for an electric conductivity of 4.2×10^{-4} S m^{-1} matches the trend of the PS particles very well (black line in Fig. 4a). The data is rescaled by taking the absolute of Re[K] and by rescaling all negative values by a factor of 0.6. This gives a good trend match between separation efficiency and particle polarizability. Employing such a (purely observational) re-scaling factor for the negative part of Re[K] is justified as negative DEP trapping is always less efficient compared to pDEP trapping as described above. Graphite particles are much more conductive and are thus experiencing positive DEP, even at much higher fluid electric conductivities than tested here. A small decrease of the separation efficiency at higher fluid

Preprints (www.preprints.org) | NOT PEER-REVIEWED | Posted: 4 December 2019 doi:10.20944/preprints201912.0055.v1

Peer-reviewed version available at Analytical and Bioanalytical Chemistry 2020; doi:10.1007/s00216-020-02557-0

conductivities is ascribed to thermal and electrothermal effects that are likely to interfere with the DEP trapping process [35], [36].

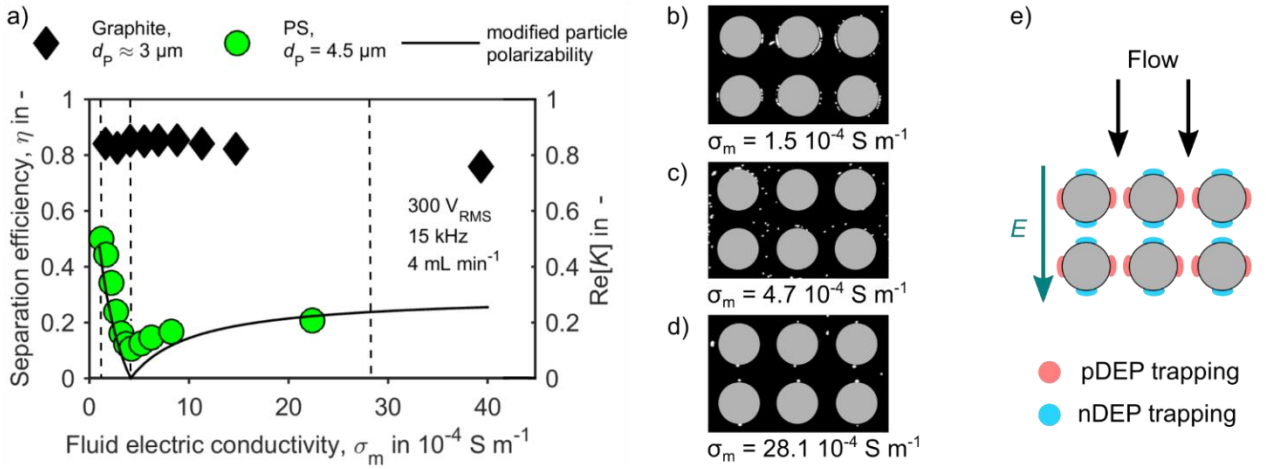

Figure 5: Separation efficiency of PS and graphite particles, each separately (not mixed) suspended in aqueous KCl solution, dependent on the fluid electrical conductivity (a). The line represents the particle polarizability (Re[*K*]) for a particle with a conductivity of 4.2 µS cm^{-1}. It shows the absolute value of Re[*K*] after Eq. (3) with the modification that negative values for Re[*K*] were multiplied by a fitting factor 0.6. The results show the potential of DEP filtration to separate particles of different conductivity. The microscopy images of observations in a microchannel (b, c, and d) illustrate the particle trapping for fluid electric conductivities (1.5×10^{-4} S m^{-1}, 4.2×10^{-4} S m^{-1}, and 28×10^{-4} S m^{-1}). A schematic of the trapping zones for positive and negative DEP in the microchannels is shown on the right (e).

D. Recovery rate and multiple filter use

To this point we have shown how particles can be removed from a suspension. Another important point that DEP filtration is capable of is the recovery of formerly trapped particles. Recovery of trapped particles is of high interest because it allows to collect particles in a highly concentrated and purified form in a suspension of choice. In all experiments that we performed we could recover 60% to 90% of the trapped particles by removing the electric field and flushing the filter at highest flow rate (11 mL min^{-1}) with 20 mL of water. After 20 mL the particle concentration at the outlet reached the initial value before trapping c_0. Figure 6 shows exemplary the normalized particle concentration in the suspension at the filter outlet. When no electric field is applied, the particle concentration is c_0. The number of trapped particles during filtration is represented by the area A_{trap} beneath c_0 times the volumetric flow rate Q, while the number of recovered particles is represented by the area A_{rec} above c_0 times the flow rate during recovery Q_{rec}. The recovery rate was then defined as the amount of recovered particles divided by the amount of formerly trapped particles, $R = (A_{rec}\ Q_{rec})/(A_{trap}\ Q)$. The factor by which particles are concentrated depends on the time DEP separation was performed prior to flushing. The relatively large deviations in recovery rate illustrate that the process is very sensitive to the filtration conditions. We believe it depends largely on the interaction between filter and particles (that can be adjusted by changing the pH value of the suspension) and on the filter surface (roughness, loading with already trapped particles etc.). This is supported by the fact that the recovery rate increased when more particles were trapped in the preceding separation period (higher load) and we found that more particles were recoverable delayed, when they had time to detach from the filter surface. This also explains why the separation efficiency remained unchanged even when the filter was reused multiple (in this study up to 30) times. Further, the flow conditions and thus the fluid flow and filter geometry have an impact on the shear force that drives particle redispersion. In conclusion, the majority of the particles can be recovered in a concentrated form with a very simple and still improvable process, flushing.

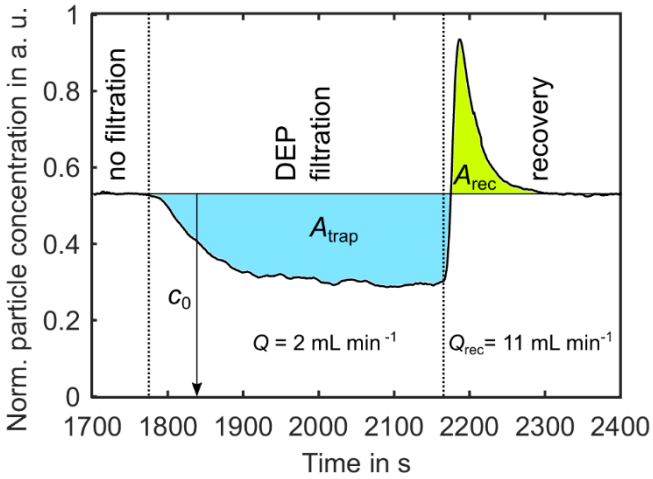

Figure 6: Exemplary plot of the normalized particle concentration in the suspension at the filter outlet during DEP filtration and subsequent particle recovery. The average particle concentration in the suspension entering the filter is c_0. The areas A_{trap} (blue) and A_{rec} (green) multiplied by the related flow rates during that times represent the normalized number of particles that was trapped and recovered. The volumetric flow during DEP filtration was 2 mL min^{-1} and was increased to 11 mL min^{-1} during recovery.

IV. CONCLUSION

Classical dielectrophoretic approaches for particle separation show high selectivity and versatility but are not able to process larger amounts of liquid as required for many bio-analytical processes (for example in the detection of circulating cancer cells) or in industrial processes like scrap recovery. This study shows that DEP filtration is capable to overcome the throughput gap between microscale and preparative or even industrial scale applications. For the first time, we achieved throughputs in the range of mL min^{-1} while still showing selective trapping and the capability to recover the majority of the trapped particles. We believe this to be a major step on the path towards industrial-scale applications of DEP separators. It should be possible to achieve throughputs of small industrial scale by simply increasing the filter cross section. According to the test setup, a throughput of 1 L min^{-1} could be processed with a filter cross section of 0.0022 m^2 and 50 L min^{-1} with 1 m^2, respectively. The presented results give further insights how the process can be adjusted by key parameters such as voltage, volumetric flow, and the structural dimensions of the filter.

In a next step, we will focus further on the selectivity of the DEP filtration process to find its possibilities and limitations. A study about selective DEP separation from a mixture of two different particles is currently on the way. A major limitation today is caused by Joule heating (heating due to electric current) that can lead to boiling or might for example cause degeneration/particle loss in biological applications. Consequently, the medium electrical conductivity (that directly correlates with the generated heat) can only be increased to a critical value that depends on how warm the suspension may become. To find ways to reduce the generated heat or how to lead it out of the process will be important. We would like to note in passing that using irregular filter structures does not allow filtration of strongly sedimenting particles because they cannot follow the suspension through the filter but sediment in regions of low fluid velocities.

DEP filtration is still in its early steps and needs to be researched further before we can use its full potential. We think, however, that DEP filtration provides unique properties that can be used to reduce costs of a variety of existing separation processes or make new and complex separation processes possible (such as material- and morphology-selective separation that have been achieved in

microscale devices). We believe that it can be of use in purely DEP-driven multistep separation processes or as an additional (preparative) tool in combination with other separation techniques. Low costs and remarkable process simplicity make DEP filtration processes attractive for research and development of test devices.

Conflicts of Interest

The authors declare that there is no conflict of interest regarding the publication of this article.

Data Availability

All data associated to this study is available from the authors upon reasonable request.

References

[1] P. R. C. Gascoyne and S. Shim, "Isolation of Circulating Tumor Cells by Dielectrophoresis," *Cancers (Basel).*, vol. 6, no. 1, pp. 545–579, Mar. 2014.

[2] R. Pethig, "Dielectrophoresis: An assessment of its potential to aid the research and practice of drug discovery and delivery," *Adv. Drug Deliv. Rev.*, vol. 65, no. 11–12, pp. 1589–1599, Nov. 2013.

[3] T. Spengler, M. Ploog, and M. Schröter, "Integrated planning of acquisition, disassembly and bulk recycling: a case study on electronic scrap recovery," in *Advanced Planning and Scheduling Solutions in Process Industry*, Berlin, Heidelberg: Springer Berlin Heidelberg, 2003, pp. 397–426.

[4] F. Du, M. Baune, A. Kück, and J. Thöming, "Dielectrophoretic Gold Particle Separation," *Sep. Sci. Technol.*, vol. 43, no. 15, pp. 3842–3855, Oct. 2008.

[5] A. Tuncuk, V. Stazi, A. Akcil, E. Y. Yazici, and H. Deveci, "Aqueous metal recovery techniques from e-scrap: Hydrometallurgy in recycling," *Miner. Eng.*, vol. 25, no. 1, pp. 28–37, Jan. 2012.

[6] C. Alix-Panabières, H. Schwarzenbach, and K. Pantel, "Circulating Tumor Cells and Circulating Tumor DNA," *Annu. Rev. Med.*, vol. 63, no. 1, pp. 199–215, Feb. 2012.

[7] Goosey M and Kellner R, "A Scoping Study End-of-Life Printed Circuit Boards Department of Trade and Industry," *Shipley Eur. Ltd.*, no. August, 2002.

[8] R. Pethig, "Review Article—Dielectrophoresis: Status of the theory, technology, and applications," *Biomicrofluidics*, vol. 4, no. 2, p. 022811, Jun. 2010.

[9] A. LaLonde, M. F. Romero-Creel, M. A. Saucedo-Espinosa, and B. H. Lapizco-Encinas, "Isolation and enrichment of low abundant particles with insulator-based dielectrophoresis," *Biomicrofluidics*, vol. 9, no. 6, p. 064113, Nov. 2015.

[10] H. A. Pohl and I. Hawk, "Separation of Living and Dead Cells by Dielectrophoresis," *Science (80-.).*, vol. 152, no. 3722, pp. 647–649, Apr. 1966.

[11] S. K. Srivastava, A. Artemiou, and A. R. Minerick, "Direct current insulator-based dielectrophoretic characterization of erythrocytes: ABO-Rh human blood typing," *Electrophoresis*, vol. 32, no. 18, pp. 2530–2540, Sep. 2011.

[12] P. R. C. Gascoyne, J. Noshari, T. J. Anderson, and F. F. Becker, "Isolation of rare cells from cell mixtures by dielectrophoresis," *Electrophoresis*, vol. 30, no. 8, pp. 1388–1398, Apr. 2009.

[13] R. Pethig, *Dielectrophoresis*. Chichester, UK: John Wiley & Sons, Ltd, 2017.

[14] H. A. Pohl, "The Motion and Precipitation of Suspensoids in Divergent Electric Fields," *J. Appl. Phys.*, vol. 22, no. 7, pp. 869–871, Jul. 1951.

[15] H. Morgan and N. G. Green, *AC Electrokinetics: Colloids and Nanoparticles*. Baldock: Research Studies Press, 2003.

[16] Y. Kang, D. Li, S. A. Kalams, and J. E. Eid, "DC-Dielectrophoretic separation of biological cells by size," *Biomed. Microdevices*, vol. 10, no. 2, pp. 243–249, 2008.

[17] G. R. Pesch *et al.*, "Recovery of submicron particles using high-throughput dielectrophoretically switchable filtration," *Sep. Purif. Technol.*, vol. 132, pp. 728–735, 2014.

[18] B. H. Lapizco-Encinas, "On the recent developments of insulator-based dielectrophoresis: A review," *Electrophoresis*, vol. 40, no. 3, pp. 358–375, Feb. 2019.

[19] G. R. Pesch *et al.*, "Bridging the scales in high-throughput dielectrophoretic (bio-)particle separation in porous media," *Sci. Rep.*, vol. 8, no. 1, p. 10480, Dec. 2018.

[20] J. Thöming, F. Du, and M. Baune, "Dielectrophoretic separation of oil-water-solid dispersions - Selectivity and particle velocity," *Fresenius Environ. Bull.*, vol. 15, no. 7, pp. 687–691, 2006.

[21] G. R. Pesch, F. Du, M. Baune, and J. Thöming, "Influence of geometry and material of insulating posts on particle trapping using positive dielectrophoresis," *J. Chromatogr. A*, vol. 1483, pp. 127–137, Feb. 2017.

[22] G. R. Pesch, L. Kiewidt, F. Du, M. Baune, and J. Thöming, "Electrodeless dielectrophoresis: Impact of geometry and material on obstacle polarization," *Electrophoresis*, vol. 37, no. 2, pp. 291–301, Jan. 2016.

[23] J. Suehiro, Guangbin Zhou, M. Imamura, and M. Hara, "Dielectrophoretic filter for separation and recovery of biological cells in water," *IEEE Trans. Ind. Appl.*, vol. 39, no. 5, pp. 1514–1521, Sep. 2003.

[24] C. Iliescu, G. Xu, F. C. Loe, P. L. Ong, and F. E. H. Tay, "A 3-D dielectrophoretic filter chip," *Electrophoresis*, vol. 28, no. 7, pp. 1107–1114, Apr. 2007.

[25] C. Iliescu, G. L. Xu, P. L. Ong, and K. J. Leck, "Dielectrophoretic separation of biological samples in a 3D filtering chip," *J. Micromechanics Microengineering*, vol. 17, no. 7, pp. S128–S136, Jul. 2007.

[26] L. Benguigui and I. J. Lin, "Dielectrophoretic Filtration of Nonconductive Liquids," *Sep. Sci. Technol.*, vol. 17, no. 8, pp. 1003–1017, Jun. 1982.

[27] I. J. Lin and L. Benguigui, "Dielectrophoretic Filtration of Liquids. II. Conducting Liquids," *Sep. Sci. Technol.*, vol. 17, no. 5, pp. 645–654, Apr. 1982.

[28] R. J. Wakeman and G. Butt, "An Investigation of High Gradient Dielectrophoretic Filtration," *Chem. Eng. Res. Des.*, vol. 81, no. 8, pp. 924–935, 2003.

[29] C. T. O'Konski, "ELECTRIC PROPERTIES OF MACROMOLECULES. V. THEORY OF IONIC POLARIZATION IN POLYELECTROLYTES," *J. Phys. Chem.*, vol. 64, no. 5, pp. 605–619, May 1960.

[30] I. Ermolina and H. Morgan, "The electrokinetic properties of latex particles: comparison of electrophoresis and dielectrophoresis," *J. Colloid Interface Sci.*, vol. 285, no. 1, pp. 419–428, May 2005.

[31] G. Schwarz, "A THEORY OF THE LOW-FREQUENCY DIELECTRIC DISPERSION OF COLLOIDAL PARTICLES IN ELECTROLYTE SOLUTION 1,2," *J. Phys. Chem.*, vol. 66, no. 12, pp. 2636–2642, Dec. 1962.

[32] W. M. Arnold, H. P. Schwan, and U. Zimmermann, "Surface conductance and other properties of latex particles measured by electrorotation," *J. Phys. Chem.*, vol. 91, no. 19, pp. 5093–5098, Sep. 1987.

[33] R. S. Chow and K. Takamura, "Effects of surface roughness (hairiness) of latex particles on their electrokinetic potentials," *J. Colloid Interface Sci.*, vol. 125, no. 1, pp. 226–236, 1988.

[34] P. R. C. Gascoyne and J. Vykoukal, "Particle separation by dielectrophoresis," *Electrophoresis*, vol. 23, no. 13, p. 1973, Jul. 2002.

[35] A. Castellanos, A. Ramos, A. González, N. G. Green, and H. Morgan, "Electrohydrodynamics and dielectrophoresis in microsystems: scaling laws," *J. Phys. D. Appl. Phys.*, vol. 36, no. 20, pp. 2584–2597, Oct. 2003.

[36] Q. Wang, N. N. Dingari, and C. R. Buie, "Nonlinear electrokinetic effects in insulator-based dielectrophoretic systems," *Electrophoresis*, vol. 38, no. 20, pp. 2576–2586, 2017.